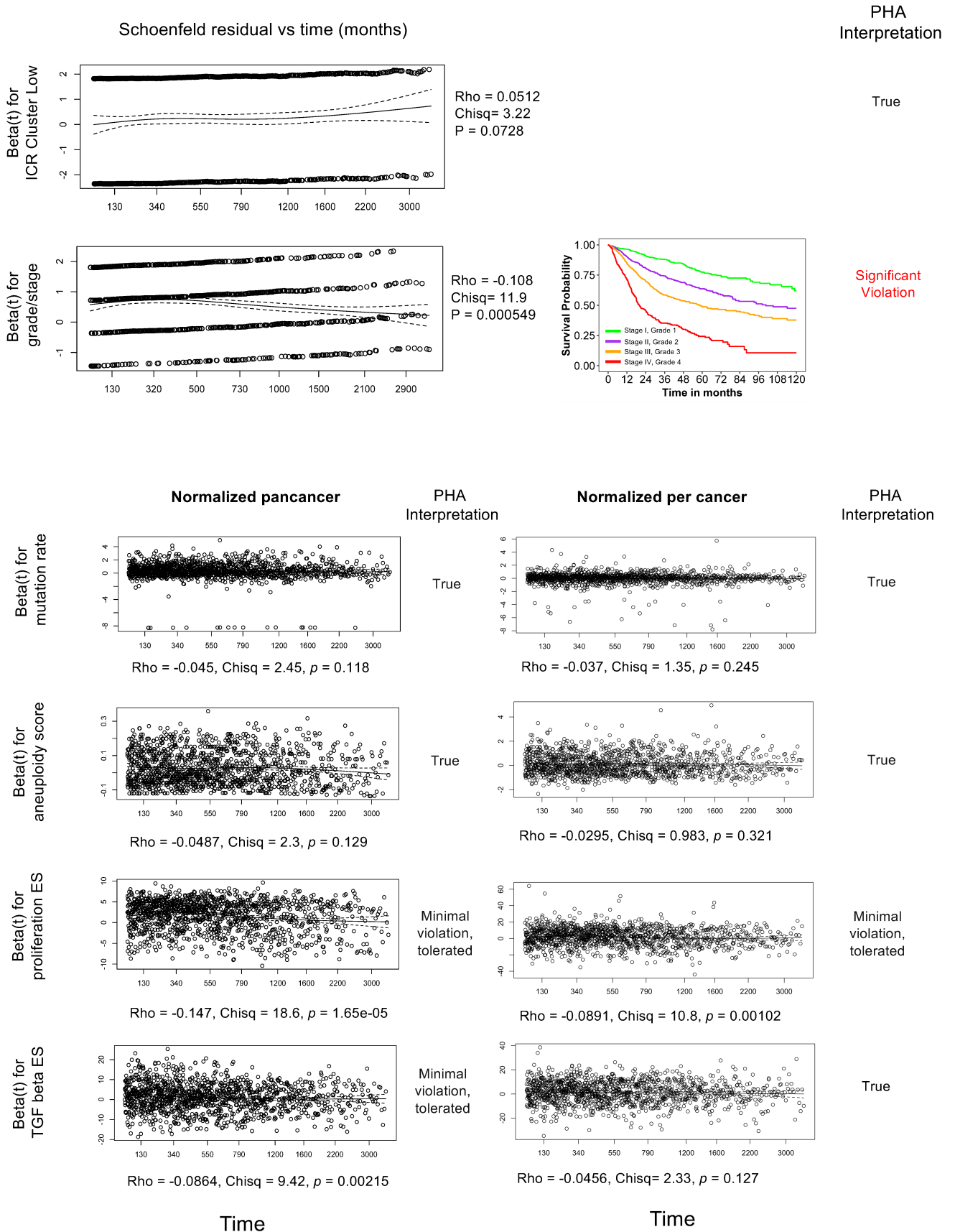


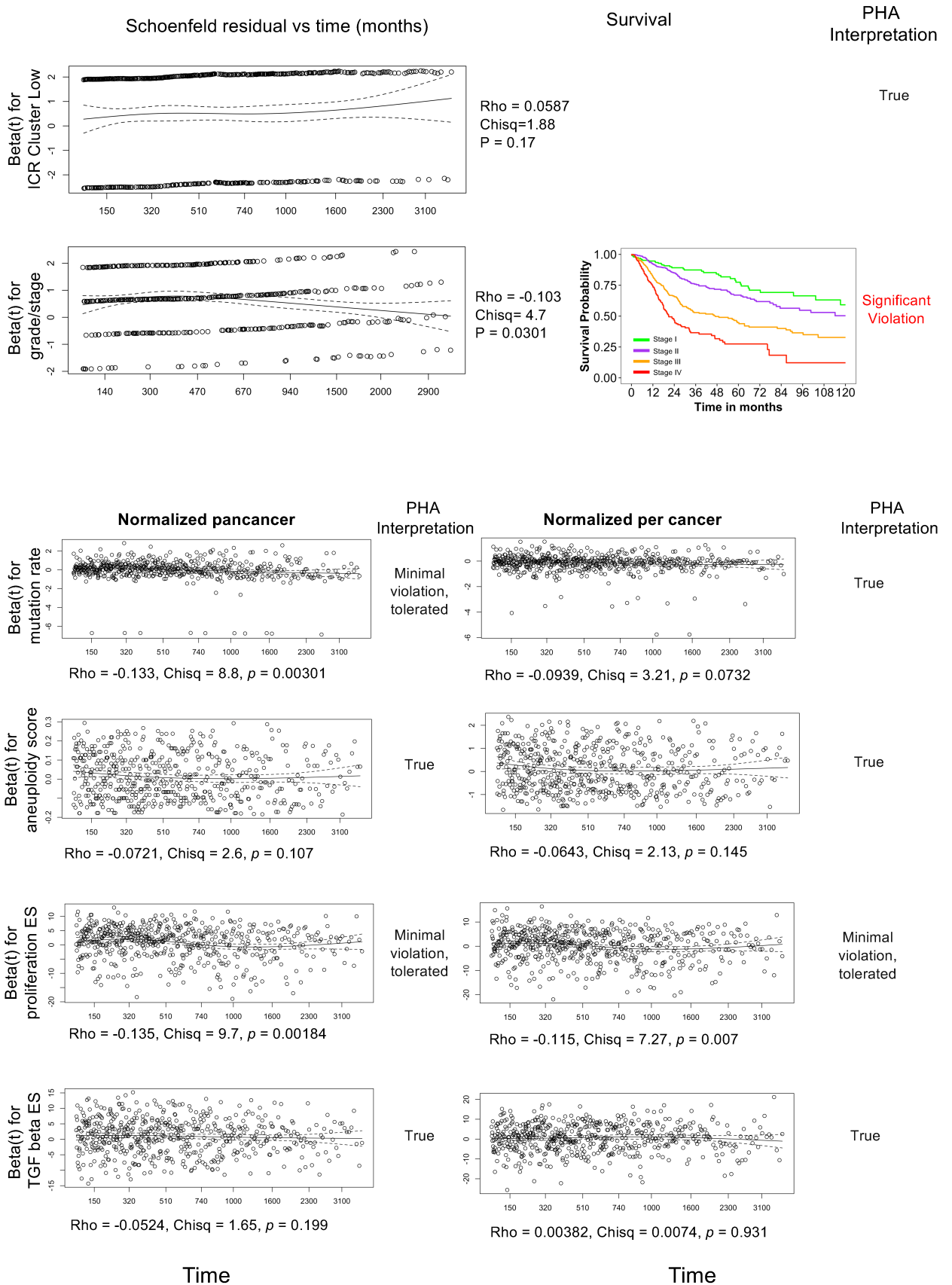
Supplementary Figure 1.1

All samples



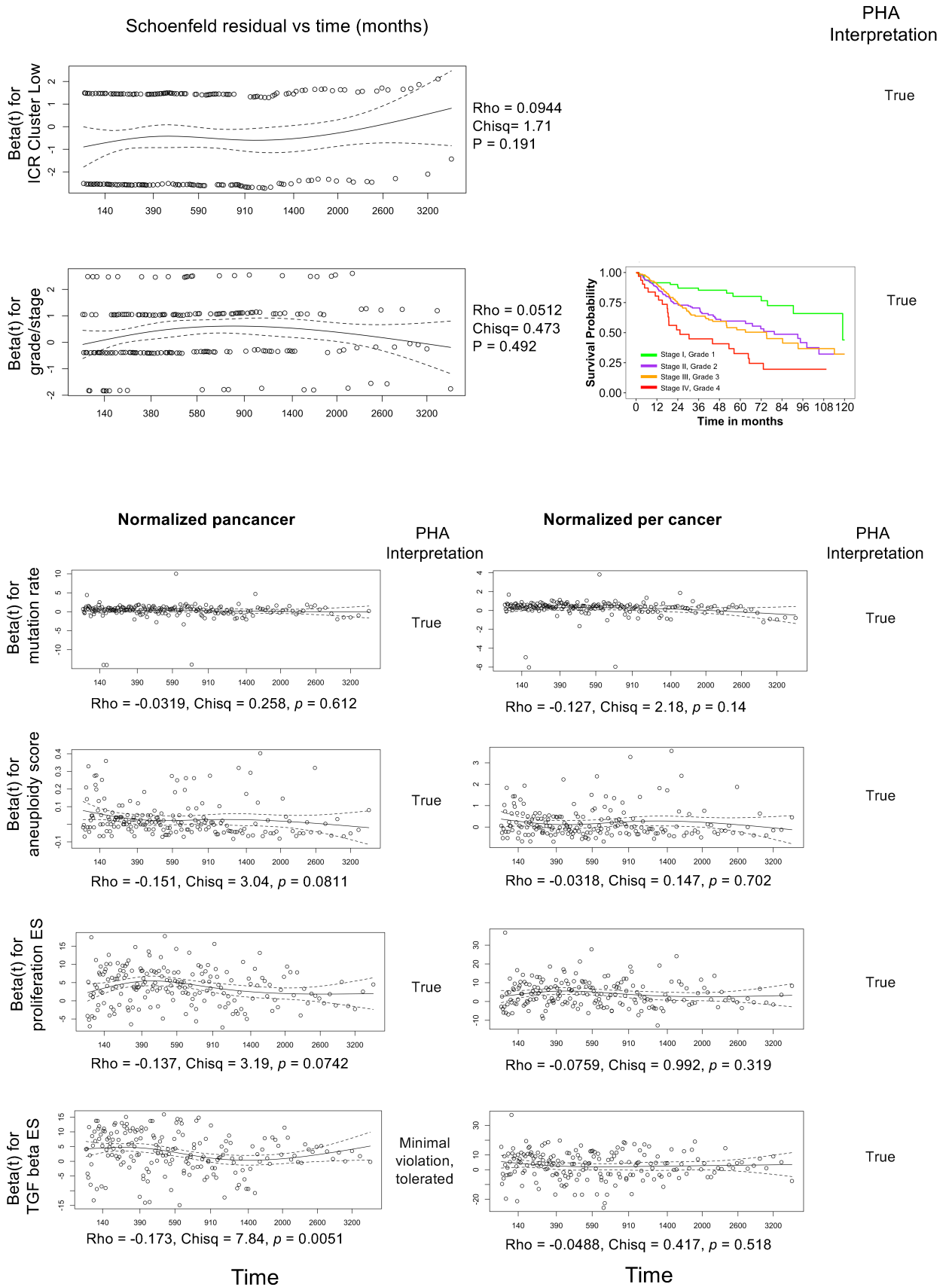
Supplementary Figure 1.2

ICR enabled



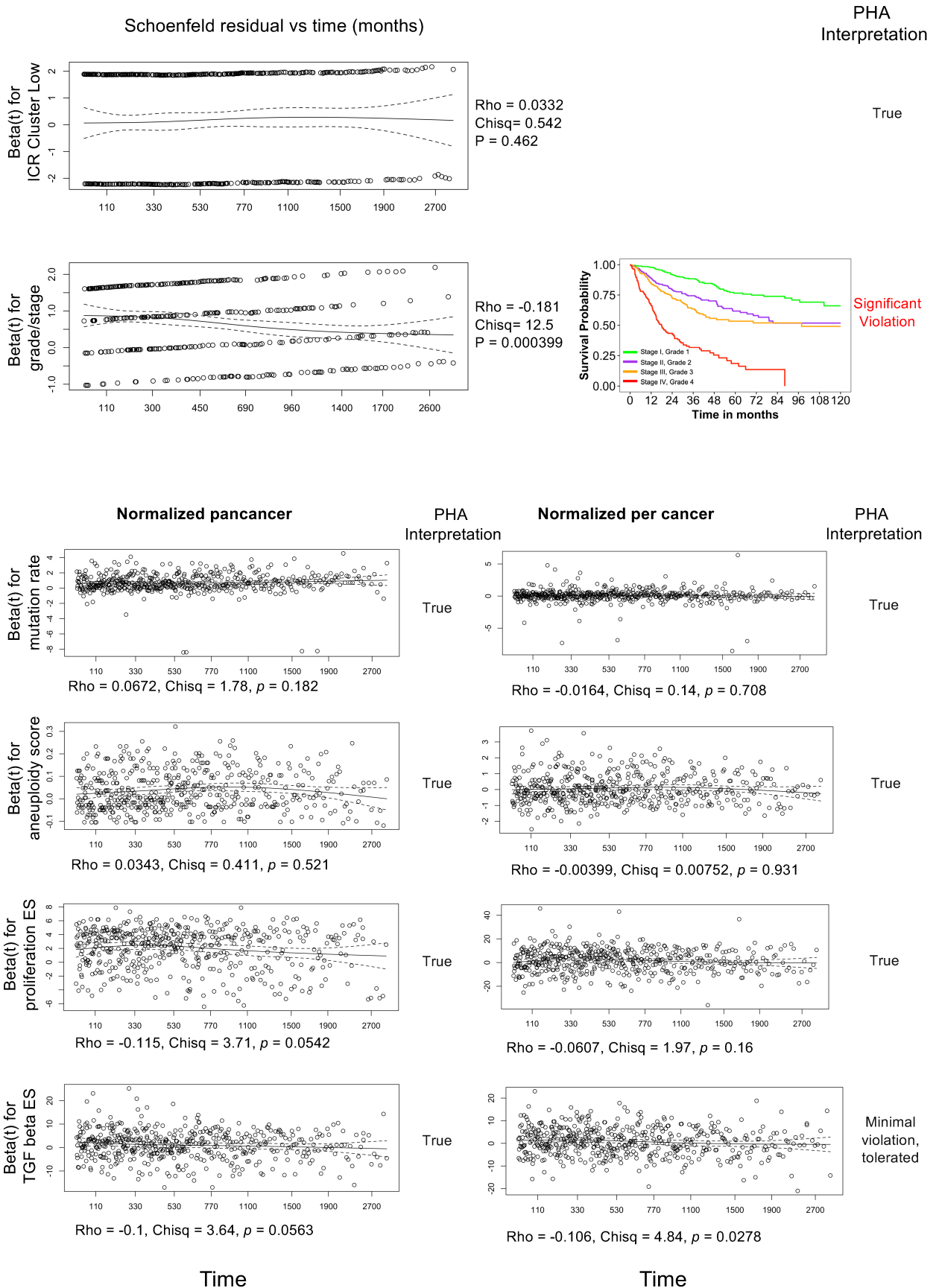
Supplementary Figure 1.3

ICR disabled



Supplementary Figure 1.4

ICR neutral



Supplementary Figure 2.2

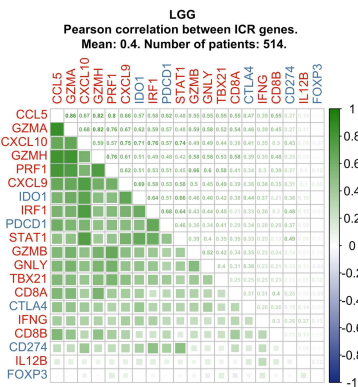


Figure: EDAsq normalized, log transformed gene expression data was obtained from TCGA, using Assembler_Panca_Normalized, filtered. Significance level of correlation is represented by the size of the squares.

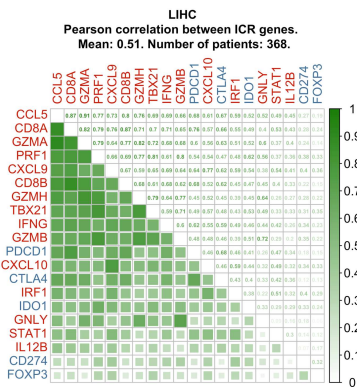


Figure: EDAsq normalized, log transformed gene expression data was obtained from TCGA, using Assembler_Panca_Normalized, filtered. Significance level of correlation is represented by the size of the squares.

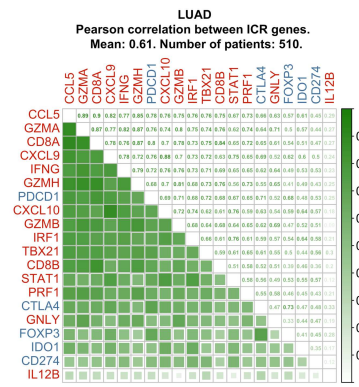


Figure: EDAsq normalized, log transformed gene expression data was obtained from TCGA, using Assembler_Panca_Normalized, filtered. Significance level of correlation is represented by the size of the squares.

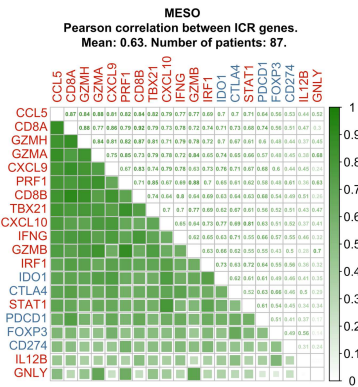


Figure: EDAsq normalized, log transformed gene expression data was obtained from TCGA, using Assembler_Panca_Normalized, filtered. Significance level of correlation is represented by the size of the squares.

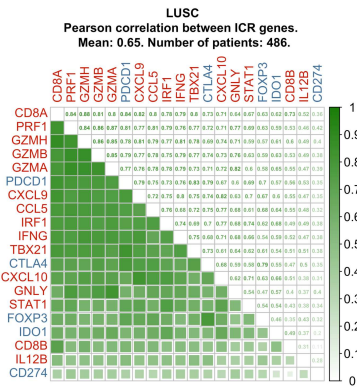


Figure: EDAsq normalized, log transformed gene expression data was obtained from TCGA, using Assembler_Panca_Normalized, filtered. Significance level of correlation is represented by the size of the squares.

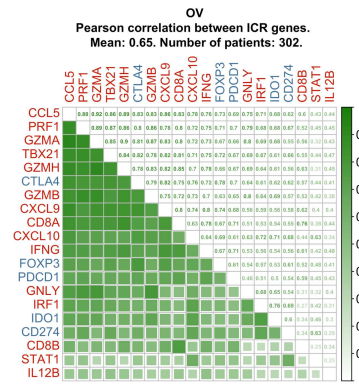


Figure: EDAsq normalized, log transformed gene expression data was obtained from TCGA, using Assembler_Panca_Normalized, filtered. Significance level of correlation is represented by the size of the squares.

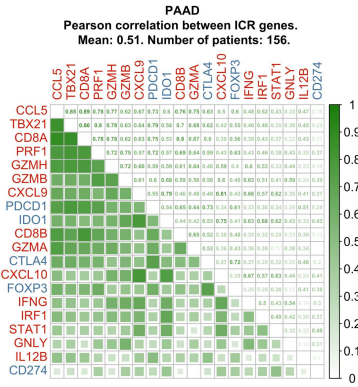


Figure: EDAsq normalized, log transformed gene expression data was obtained from TCGA, using Assembler_Panca_Normalized, filtered. Significance level of correlation is represented by the size of the squares.

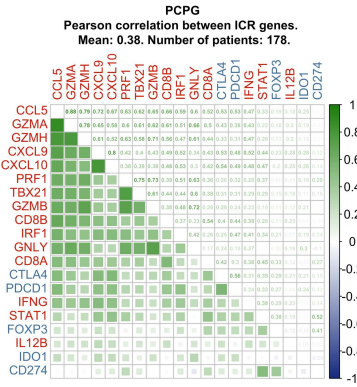


Figure: EDAsq normalized, log transformed gene expression data was obtained from TCGA, using Assembler_Panca_Normalized, filtered. Significance level of correlation is represented by the size of the squares.

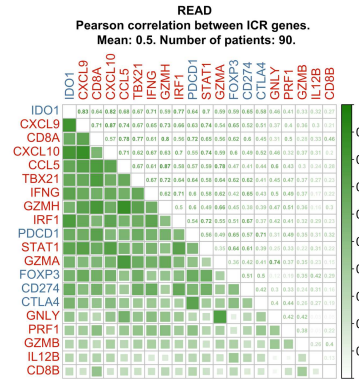


Figure: EDAsq normalized, log transformed gene expression data was obtained from TCGA, using Assembler_Panca_Normalized, filtered. Significance level of correlation is represented by the size of the squares.

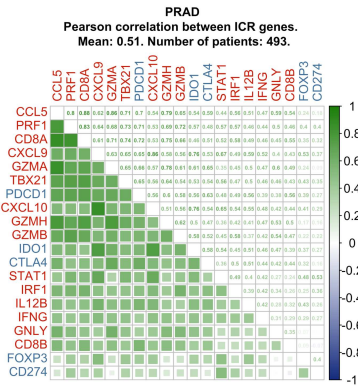


Figure: EDAsq normalized, log transformed gene expression data was obtained from TCGA, using Assembler_Panca_Normalized, filtered. Significance level of correlation is represented by the size of the squares.

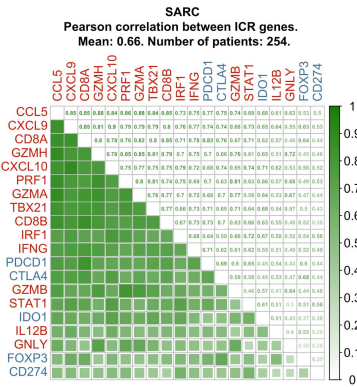


Figure: EDAsq normalized, log transformed gene expression data was obtained from TCGA, using Assembler_Panca_Normalized, filtered. Significance level of correlation is represented by the size of the squares.

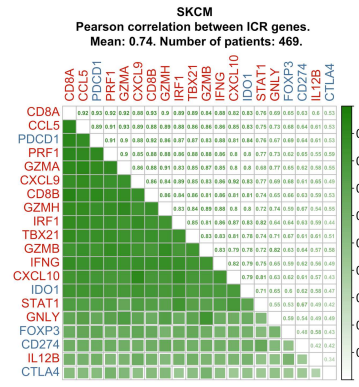
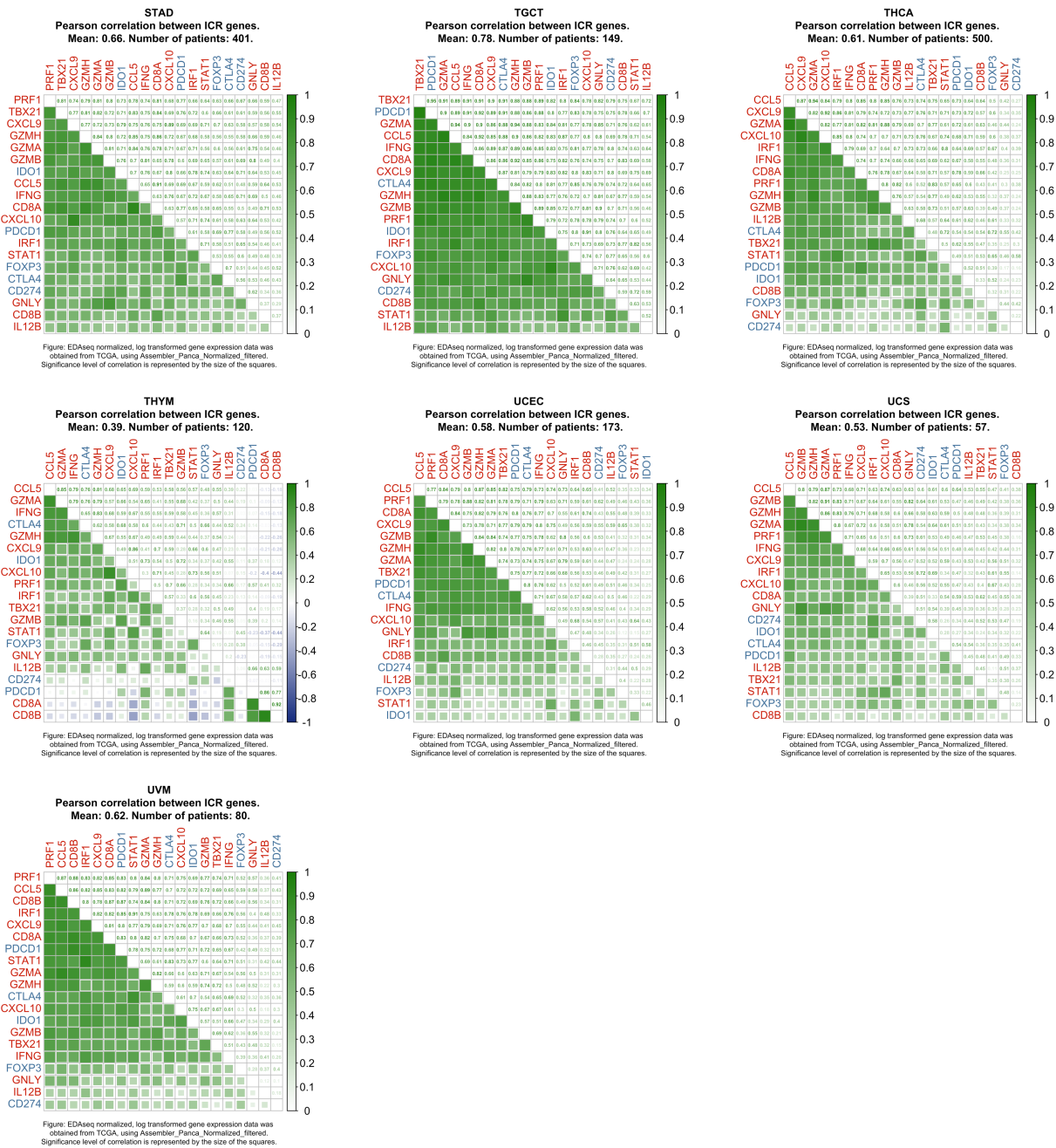
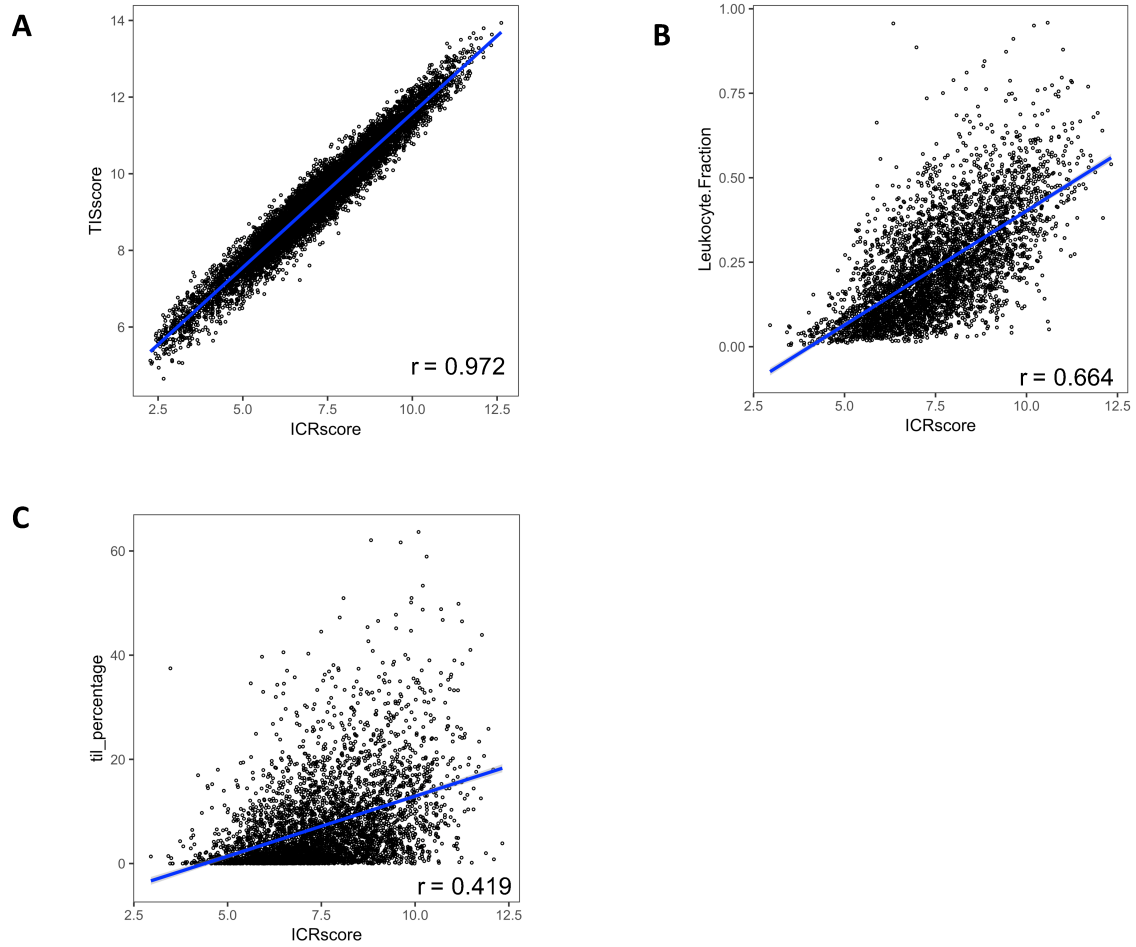


Figure: EDAsq normalized, log transformed gene expression data was obtained from TCGA, using Assembler_Panca_Normalized, filtered. Significance level of correlation is represented by the size of the squares.

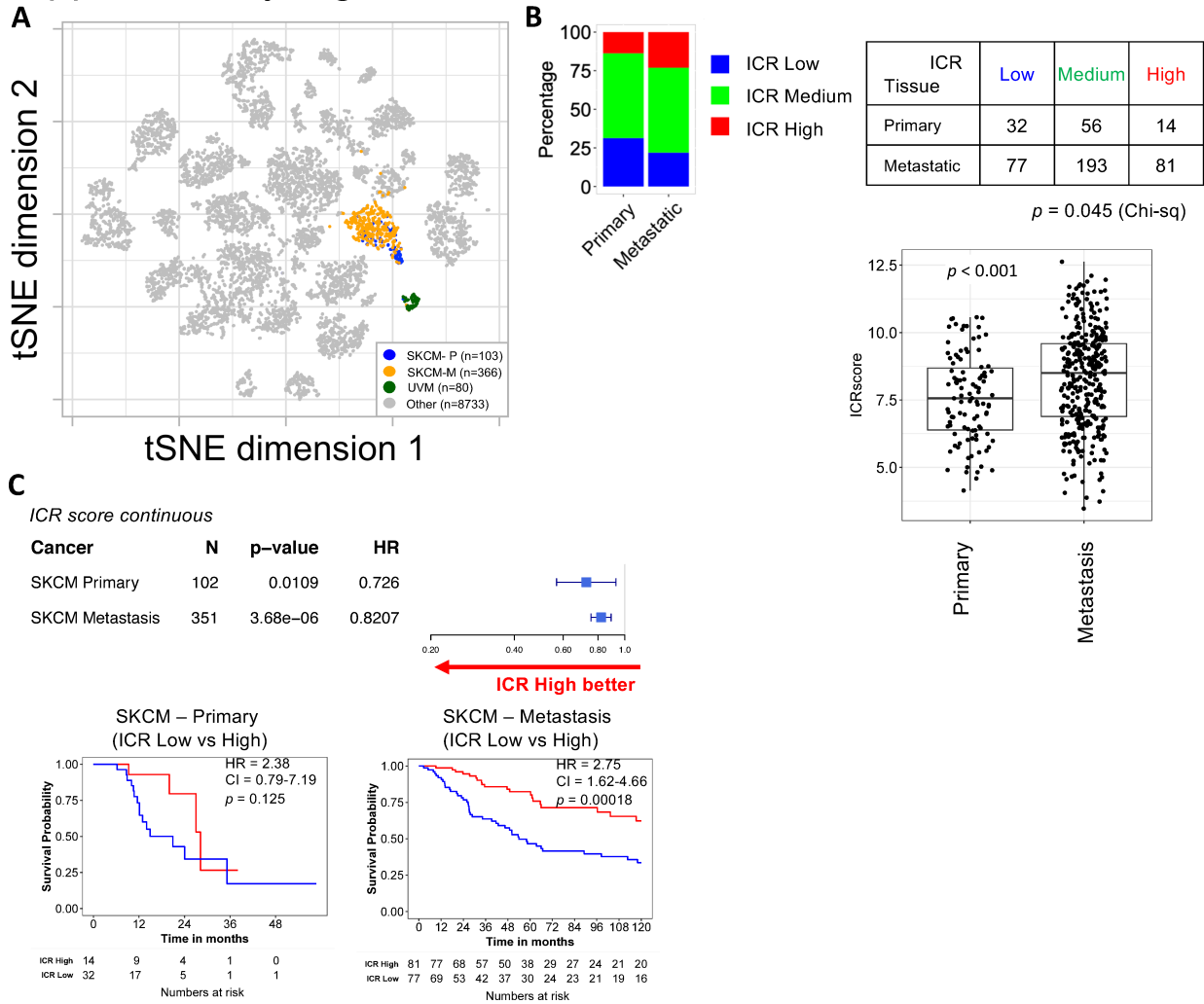
Supplementary Figure 2.3



Supplementary Figure 3



Supplementary Figure 4



Supplementary Figure 5

A

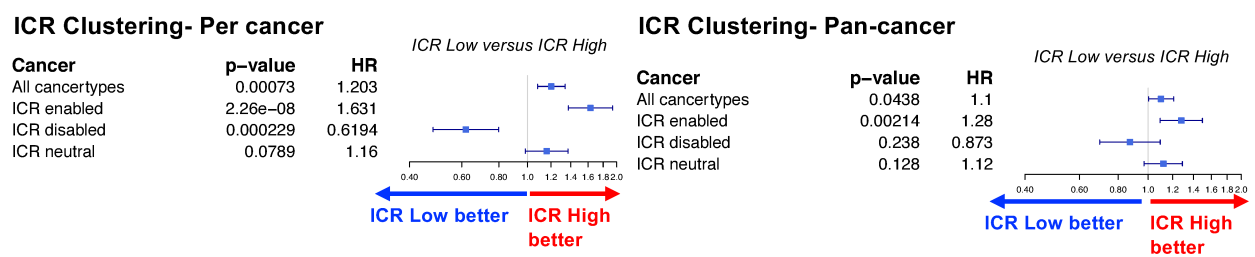


B

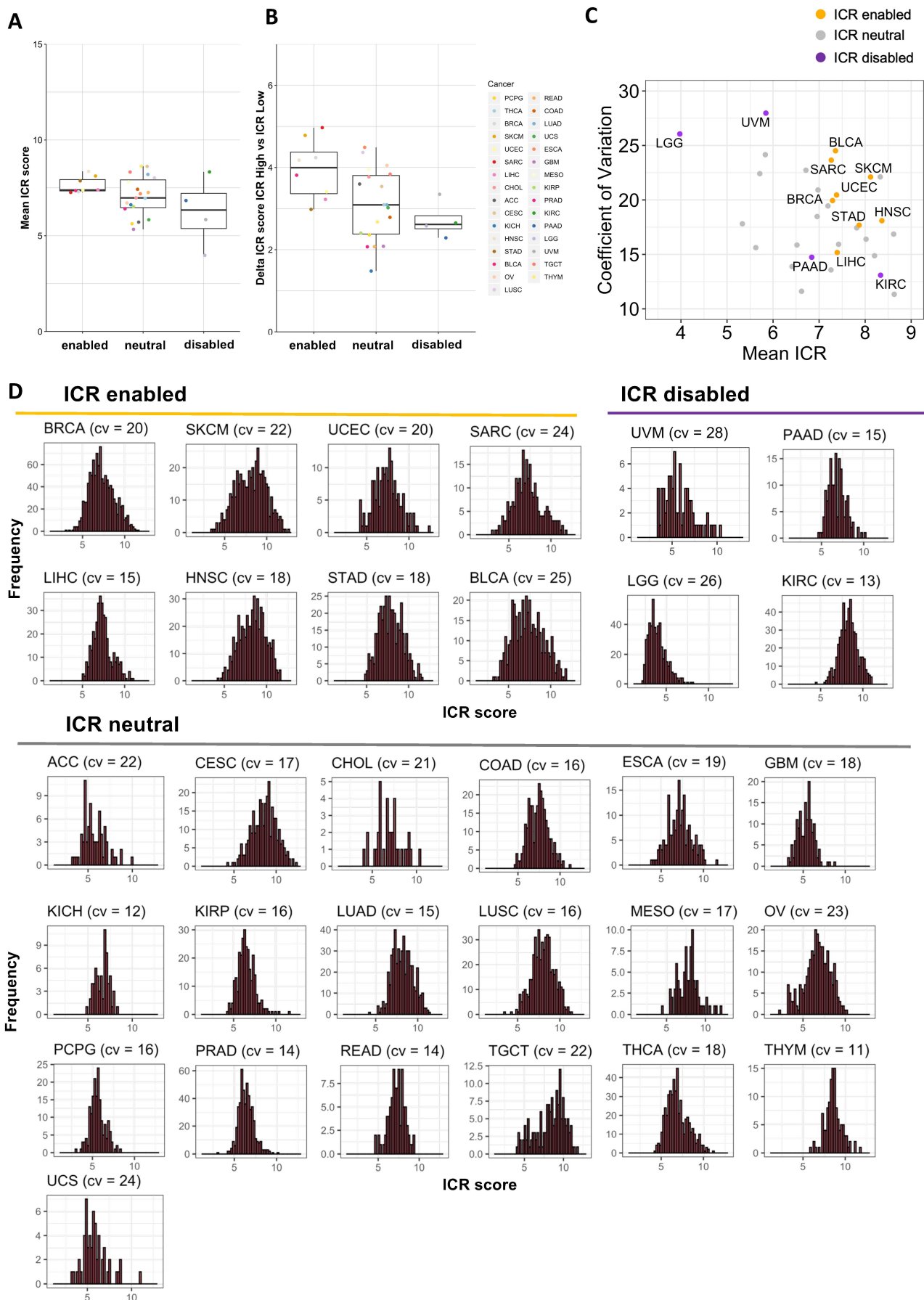
Cancer	N	N ICR High	N ICR Low	p-value	HR
UVM	80	13	47	0.000333	0.142
PAAD	156	41	32	0.332	0.733
STAD	401	249	38	0.995	1
BLCA	404	194	114	0.155	1.29
BRCA	1082	473	236	0.111	1.41
SARC	254	111	62	0.0929	1.53
HNSC	514	373	41	0.0647	1.54
SKCM	469	312	62	1.78e-05	2.29
LIHC	368	173	33	0.00292	2.43
UCEC	173	90	33	0.0326	2.62

ICR Low versus ICR High

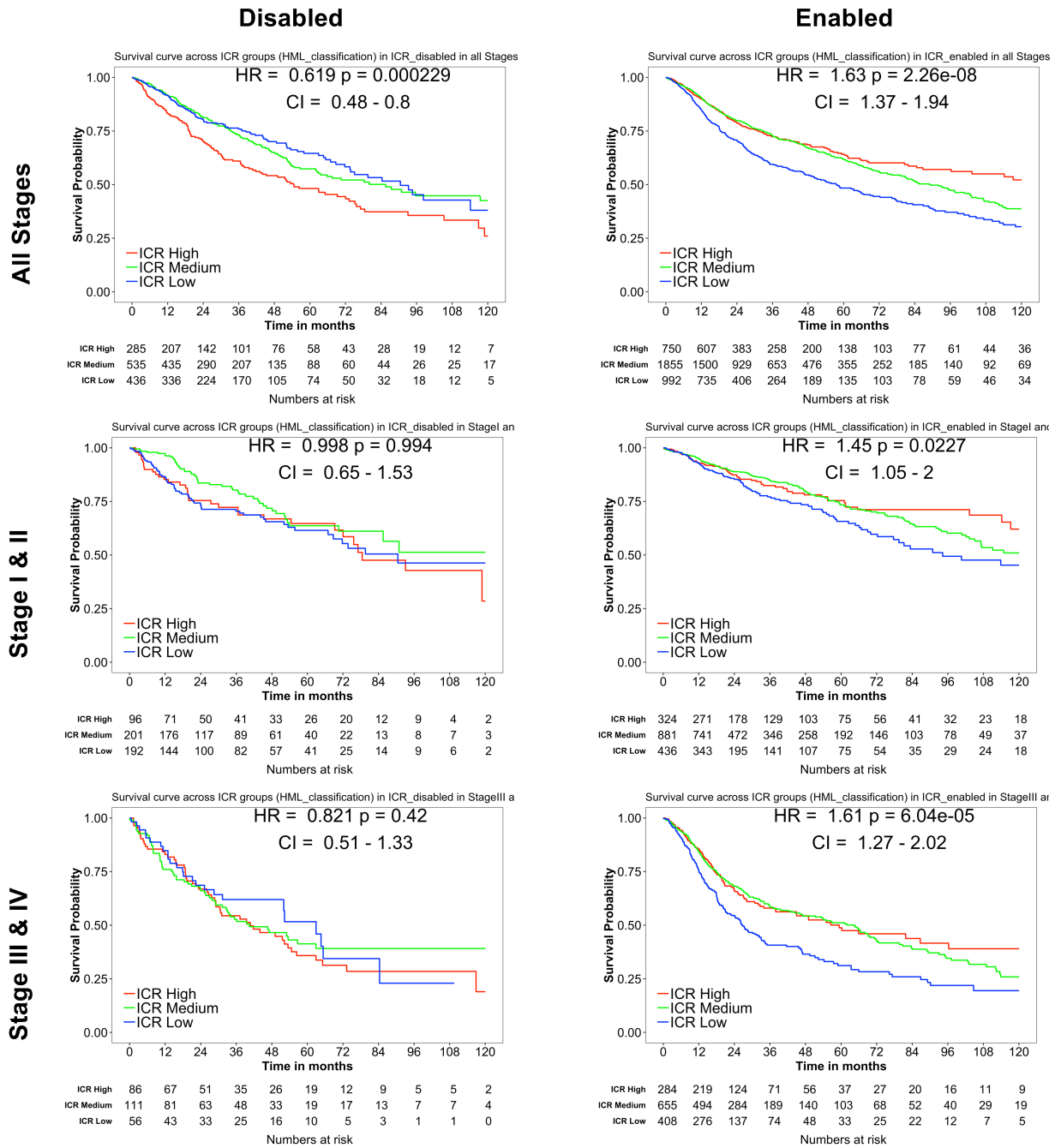
C



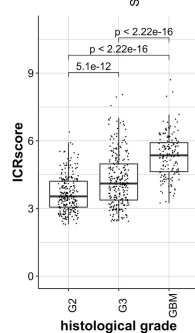
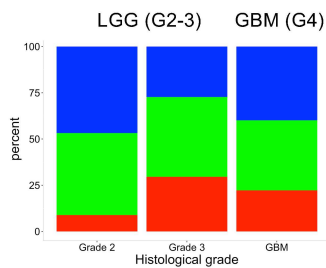
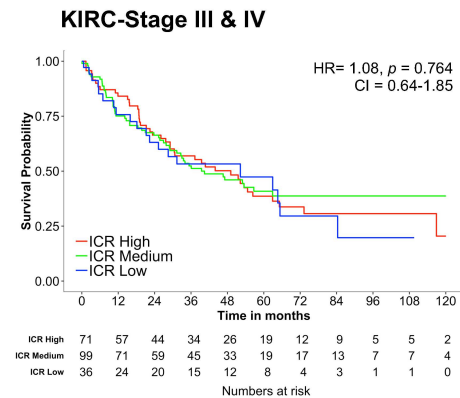
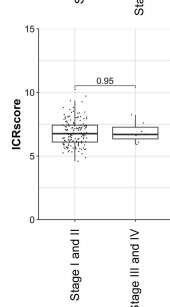
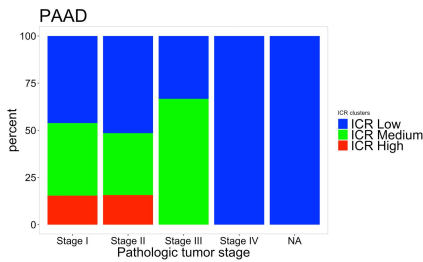
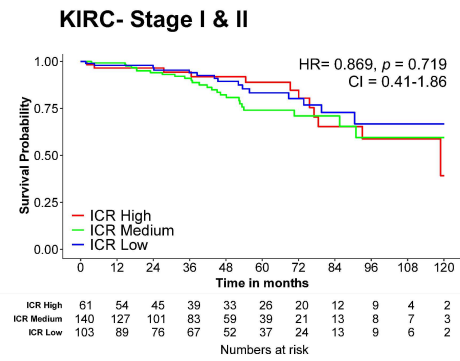
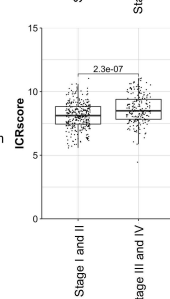
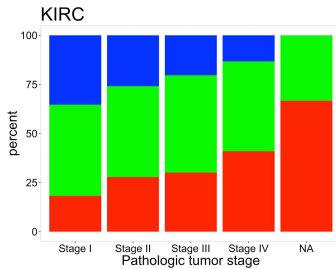
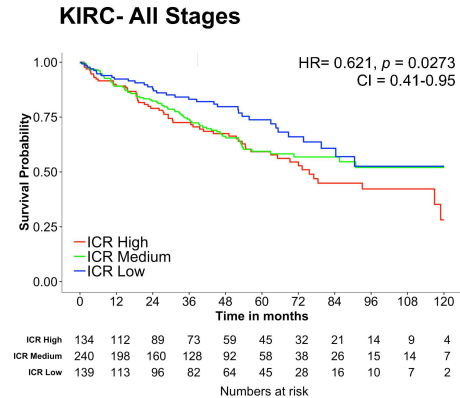
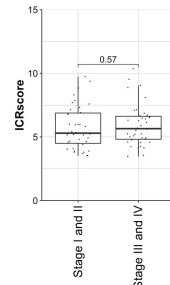
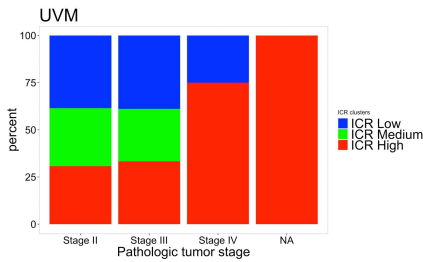
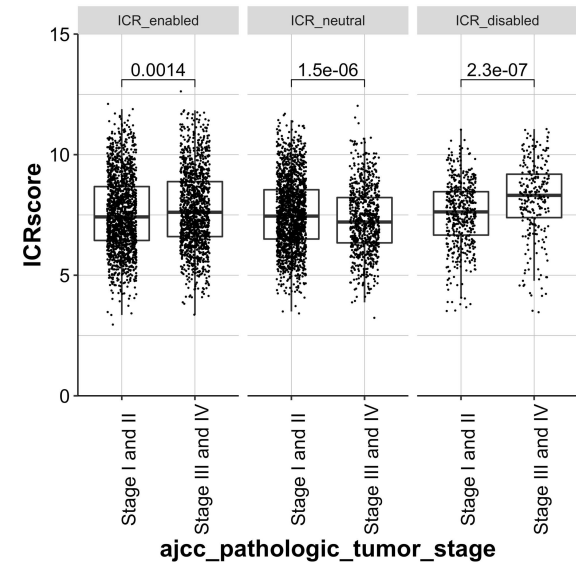
Supplementary Figure 6



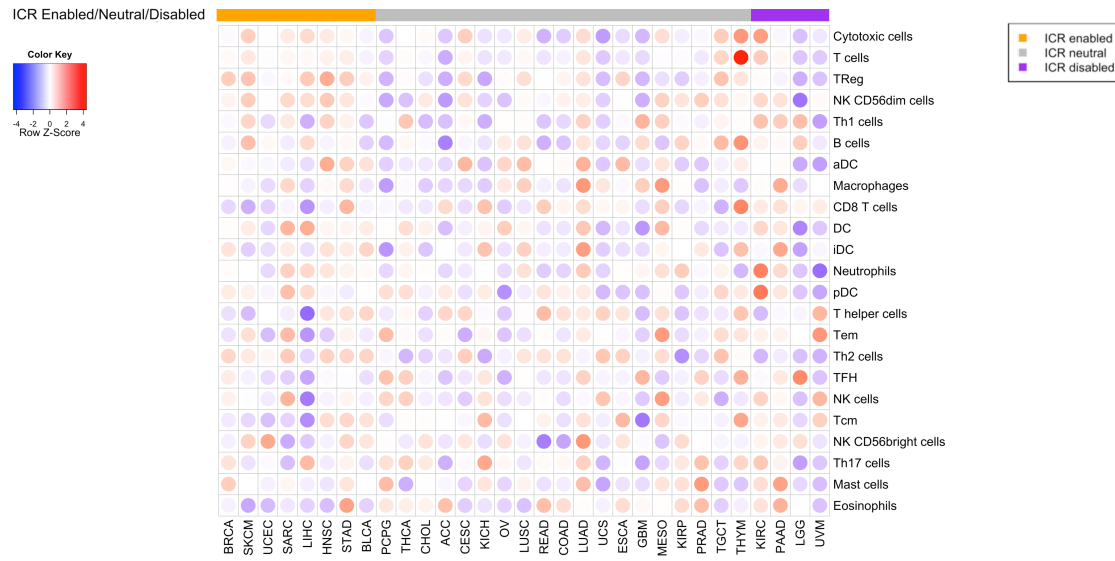
Supplementary Figure 7.1



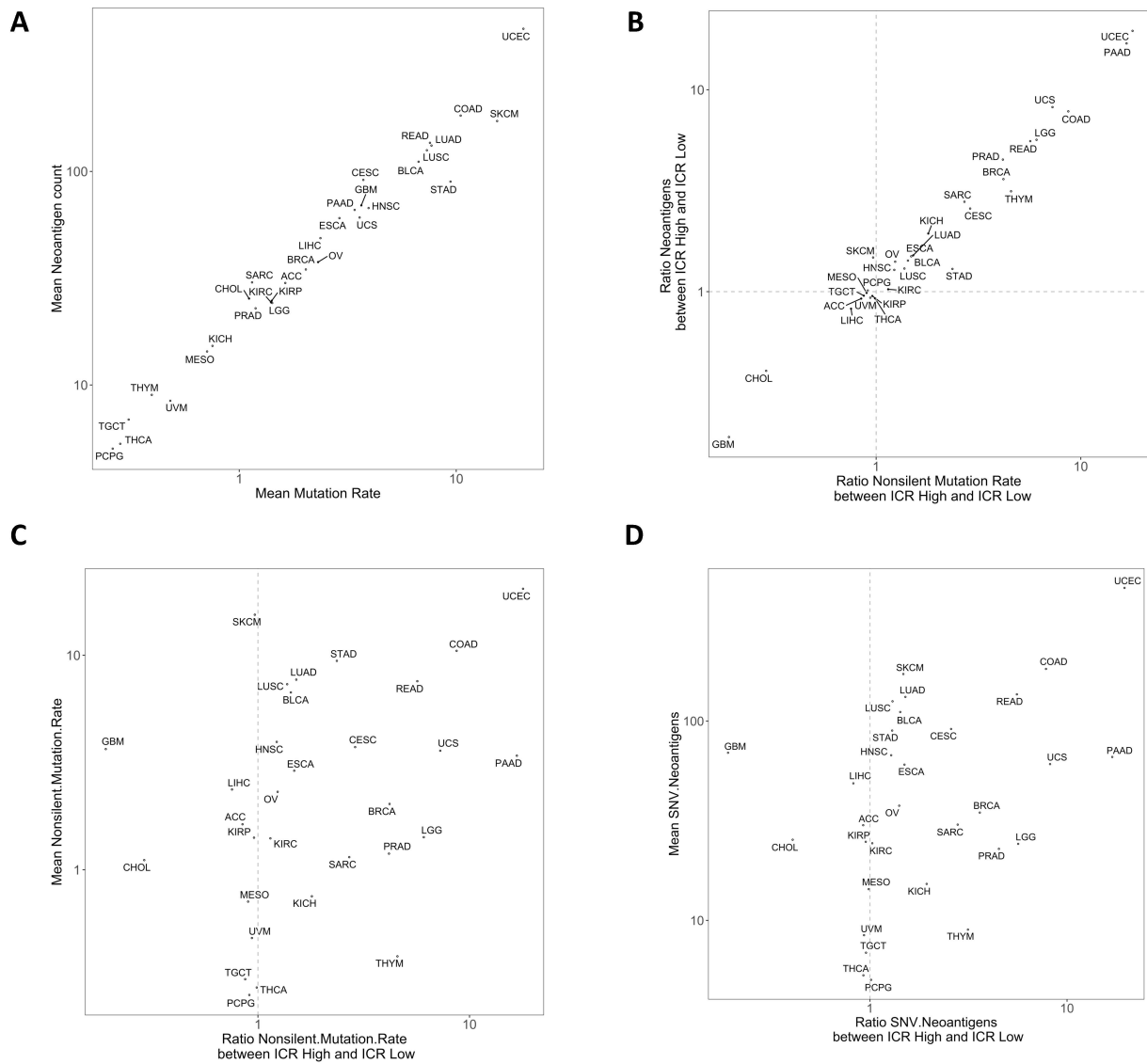
Supplementary Figure 7.2



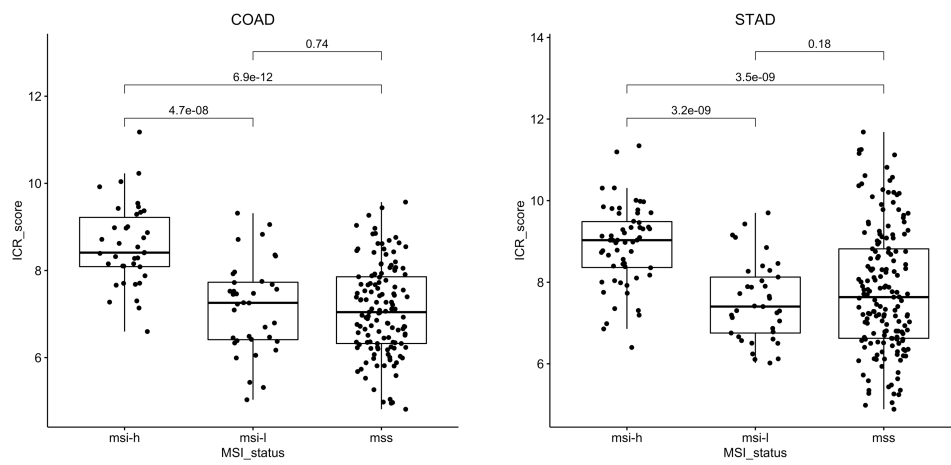
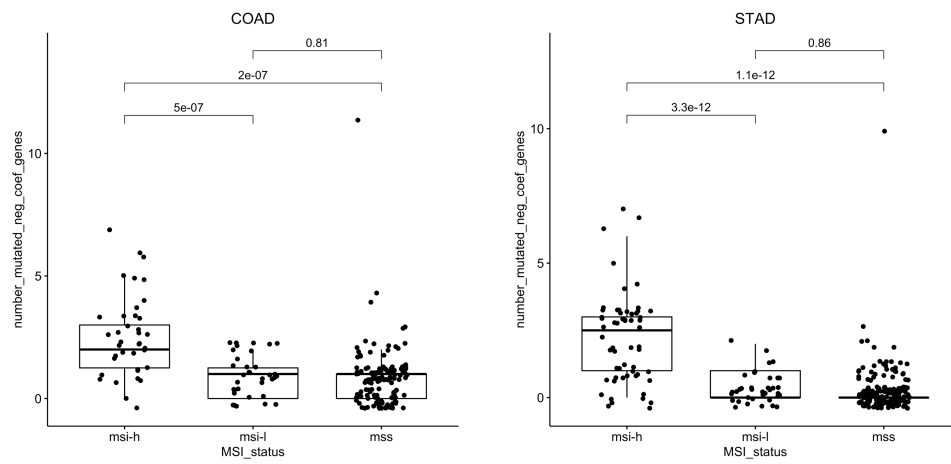
Supplementary Figure 8



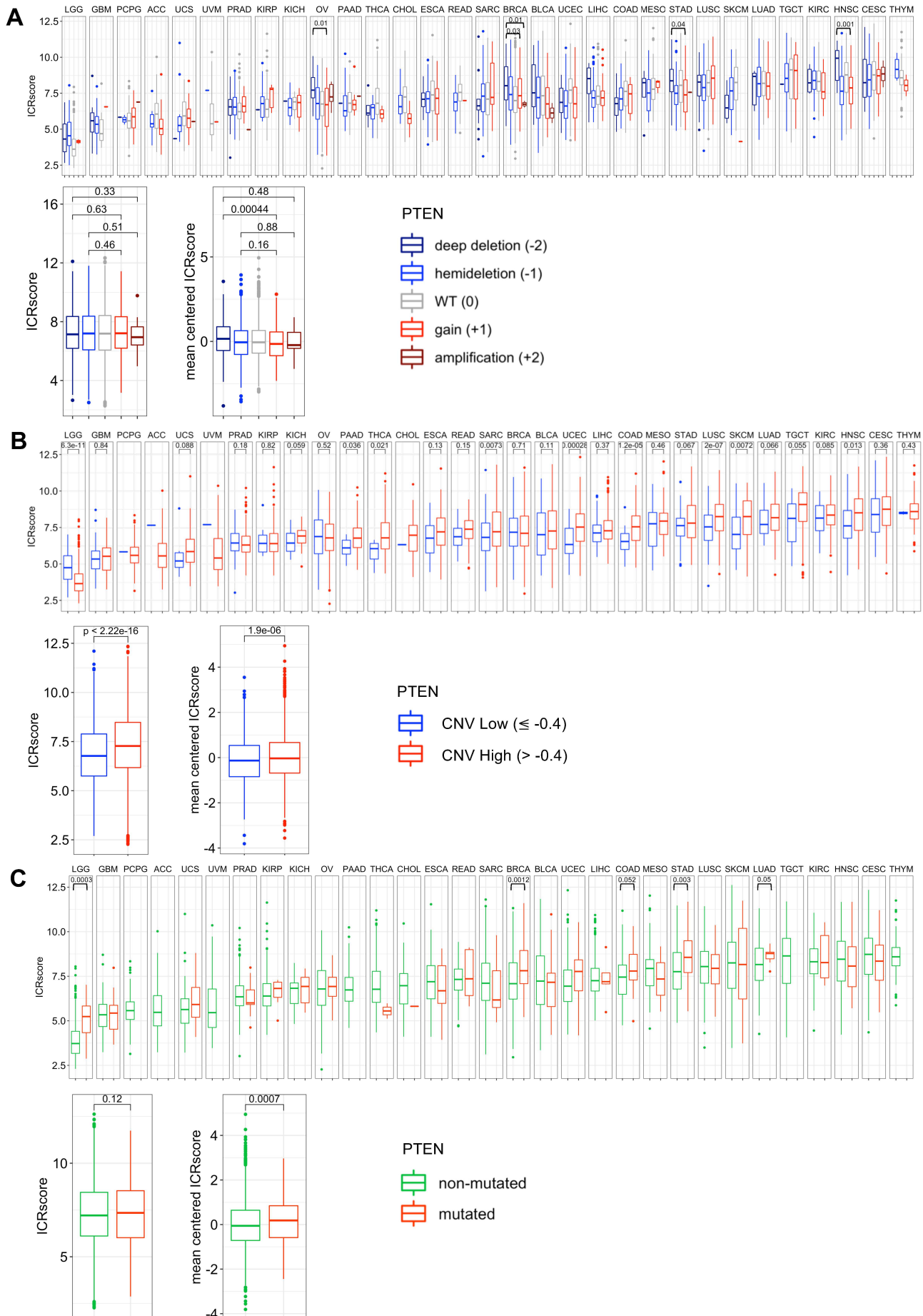
Supplementary Figure 9



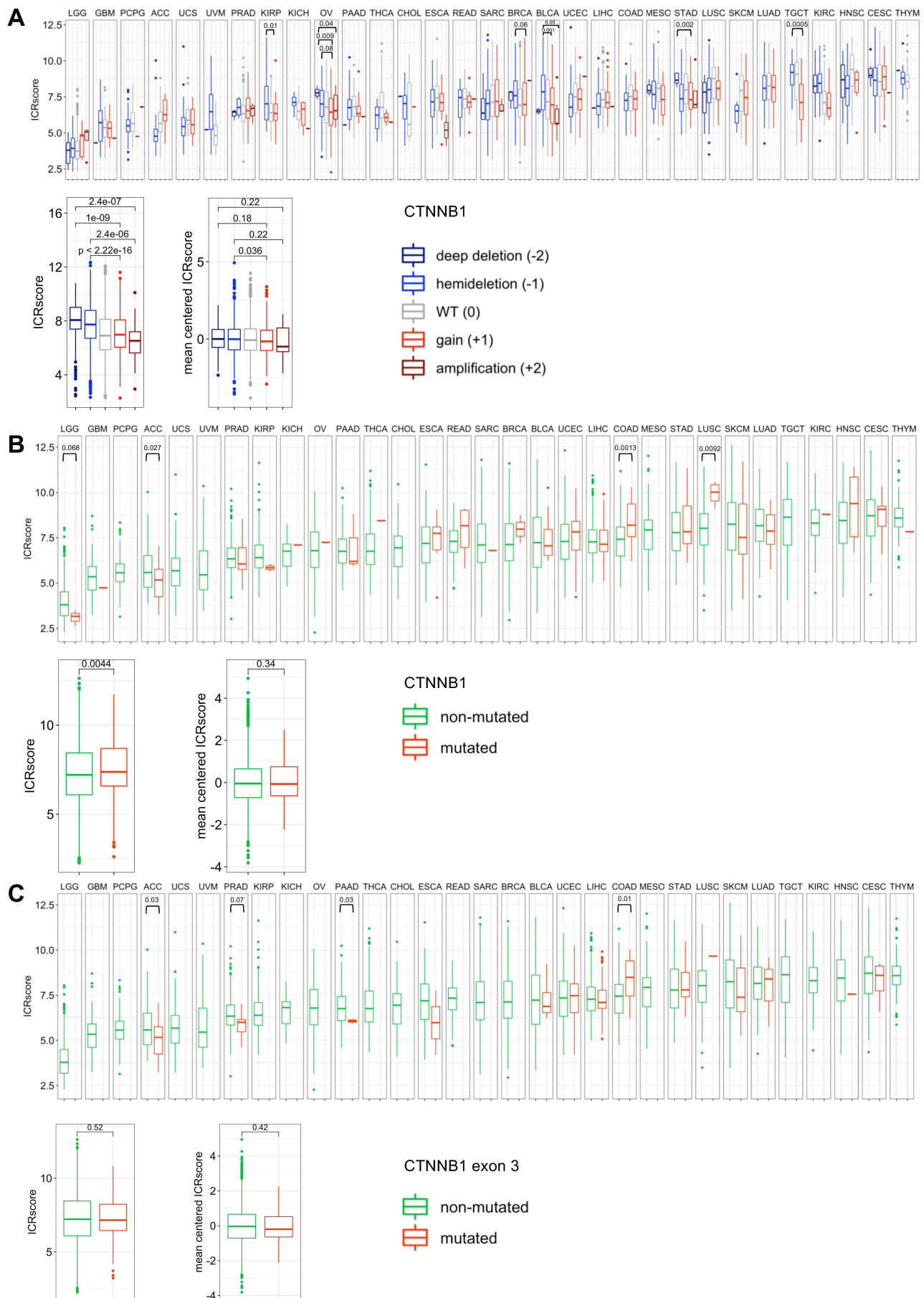
Supplementary Figure 10

A**B**

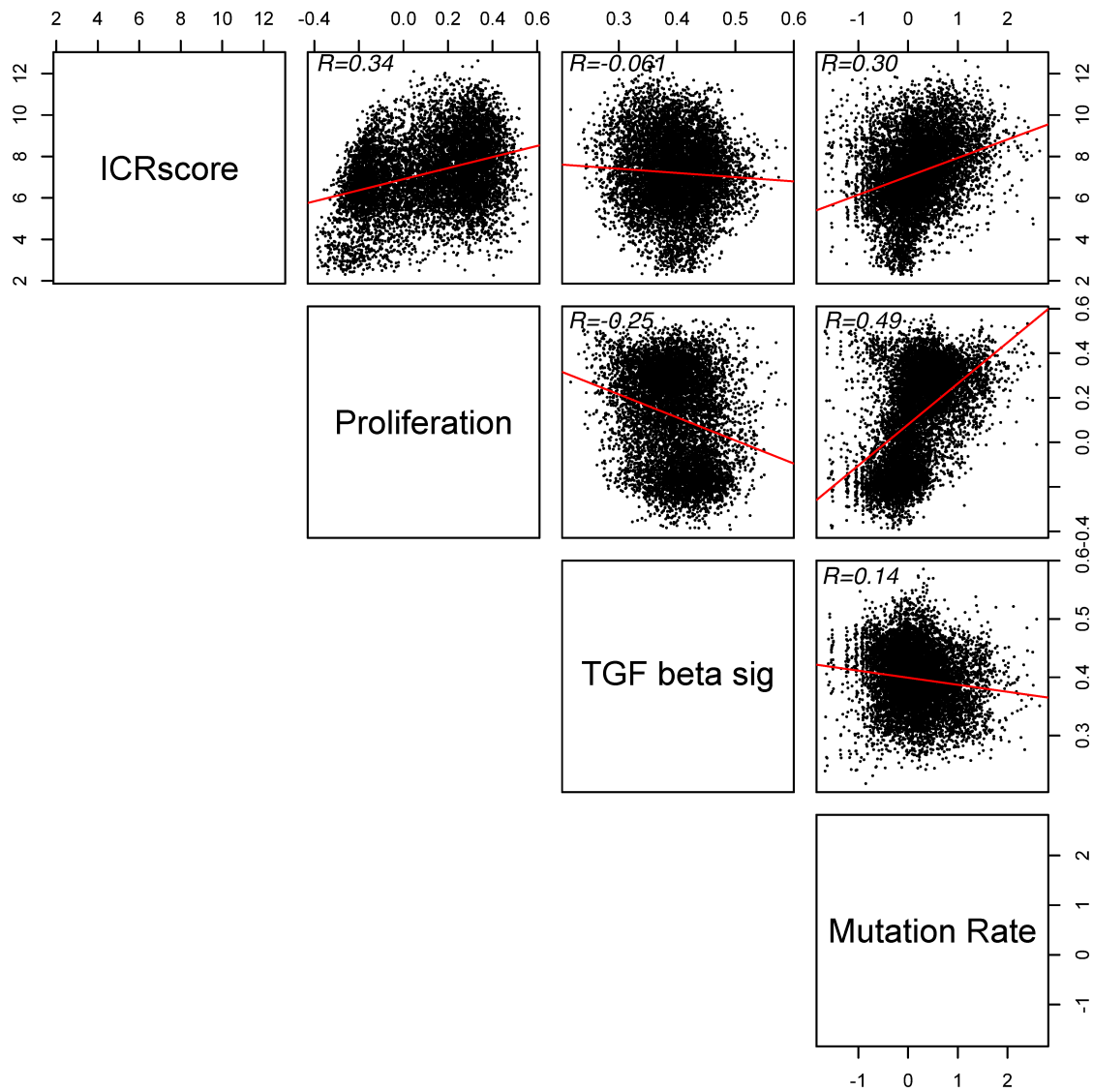
Supplementary Figure 12



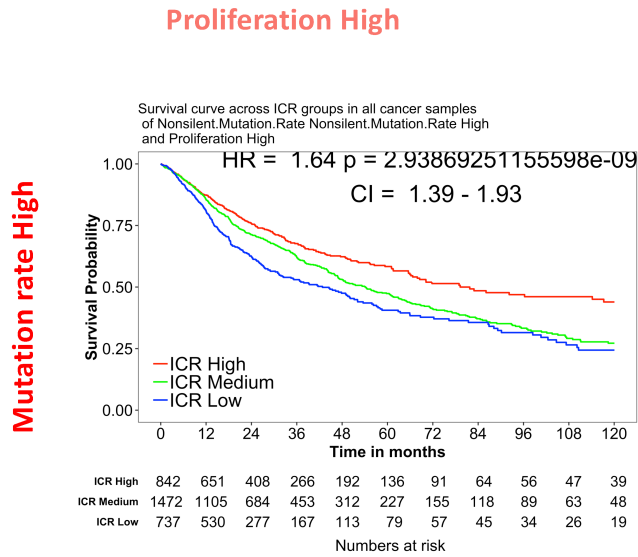
Supplementary Figure 13



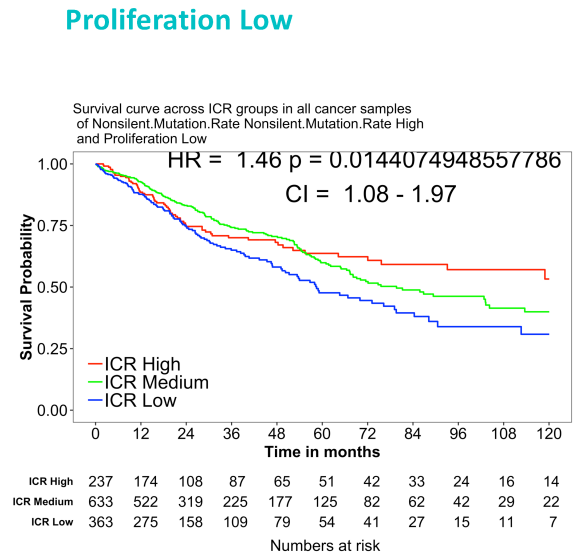
Supplementary Figure 14



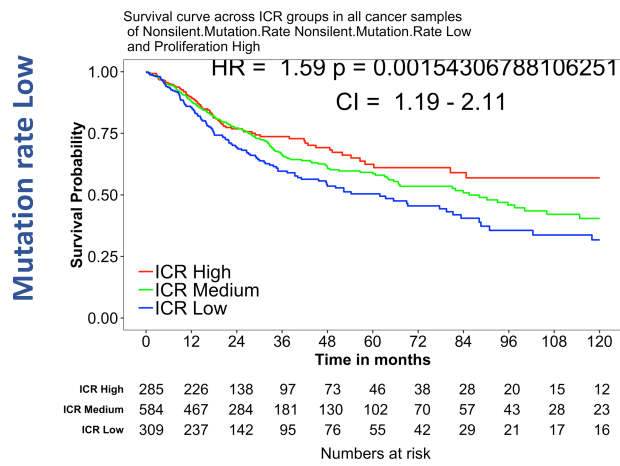
Supplementary Figure 15



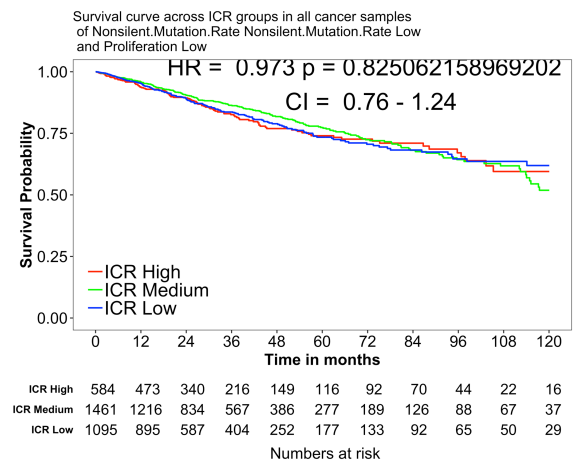
N = 3051



N = 1233



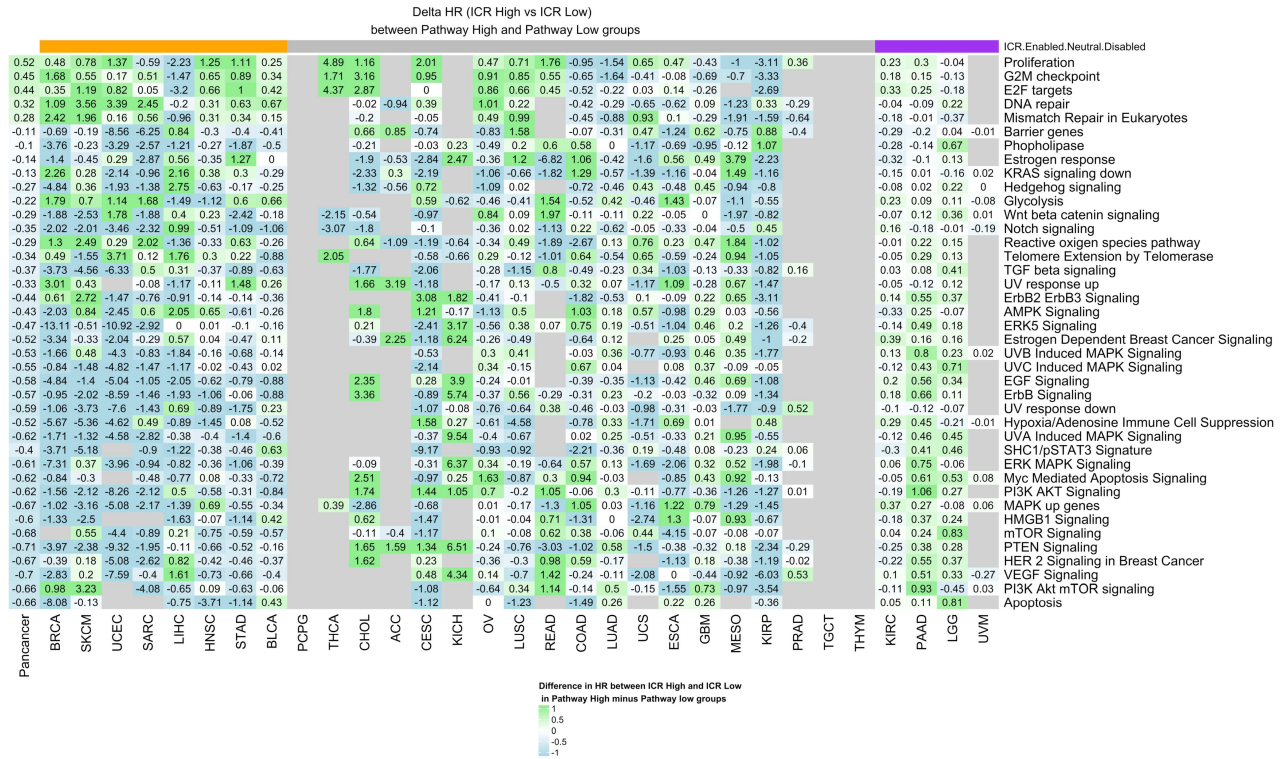
N = 1178



N = 3140

Supplementary Figure 16.2

C Analysis of Delta HR Pathway High – HR Pathway Low



Supplementary Figure 1: Scaled Schoenfeld residuals plotted against the transformed survival time as a dependent variable for each variable included in multivariate Cox models (*left panels*). Statistics of the Pearson product-moment correlation (ρ) between the Schoenfeld residuals and the transformed (log) survival time calculated with the *cox.zph* R function are indicated. Kaplan Meier curves visualizing survival probability over time across the different groups (*middle panels*). To enable visualization, continuous variables mutation rate, aneuploidy score, proliferation ES, and TGF-beta ES are dichotomized in High and Low groups, $>$ median, and \leq median, respectively. Interpretation of proportional hazards assumption test (*right panels*). Results are presented for multivariate models including all samples (*page 1*), ICR enabled samples only (*page 2*), ICR disabled samples only (*page 3*), and ICR neutral samples only (*page 4*). ES: enrichment score.

Supplementary Figure 2: Pearson correlation between RNA-seq expression values of ICR genes for each of the 31 cancer types.

Supplementary Figure 3: Scatterplot showing correlation between ICR score and TIS score(5) (**A**), ICR score and leukocyte fraction (**B**), and ICR score and TIL percentage (**C**). Leukocyte fraction and TIL percentage values were obtained from Thorsson *et al* (7). Each dot represents a single sample.

Supplementary Figure 4: A. 2D TSNE plot of pan-cancer normalized, log₂ transformed gene expression of 9282 samples across 31 cancer types. Samples of each cancer type tend to cluster together. Plot is annotated for skin cutaneous melanoma primary (SKCM-P), and metastatic (SKCM-M) cutaneous melanoma, uveal melanoma (UVM), and other, non-melanoma samples. **B.** Stacked barchart showing distribution of immunological constant of rejection (ICR) clusters within SKCM primary and metastatic samples, assigned within SKCM cancer type (*upper left panel*). Contingency table of number of samples in each ICR and tissue category (*upper right panel*). Box plot of ICR score in in primary vs metastatic tumors (p is from t-test). **C.** Forest plot of cox proportional hazards model with ICR score as continuous variable in SKCM-P and SKCM-M categories (*upper panel*). Kaplan Meier curves and hazard ratios (HR) for death of ICR Low versus ICR High samples in SKCM-P and SKCM-M categories (*lower panel*). CI: 95% confidence interval.

Supplementary Figure 5: Comparison of ICR clustering per cancer with pan-cancer clustering. As exploratory analysis, ICR assignment was determined using the whole matrix (Pan-cancer ICR clustering). A. Proportion of samples assigned to ICR Low-, Medium, and High groups by cancer type, in per cancer clustering (*upper panel*) and pan-cancer ICR

clustering (*lower panel*). Cancer types are sorted by ICR enabled, ICR neutral, and ICR disabled categories. B. Forest plot showing hazard ratio (HR) of death in pan-cancer ICR Low versus pan-cancer ICR High groups in ICR disabled (*purple*) and ICR enabled (*orange*) cancer types. As compared to per-cancer clustering analysis (see result section), similar results in term of survival were observed in 7 out of 8 enabled cancers (the only exception being observed in STAD [HR=1], due to relatively high ICR scores and low dynamic range, resulting in a limited number of samples assigned to ICR low category). Similar considerations apply to the analysis of the ICR-disabled tumors, in which the low number of ICR High and Low sample as per pan-cancer clustering, N=2 and N=9, in LGG and KIRC, respectively, prevented survival analysis in those tumor types. C. Aggregate analysis for ICR-enabled and ICR-disabled tumor returned similar results as compared to the ones obtained using the per-cancer ICR clustering. The forest plots represent HR for death, ICR Low versus ICR High, across all cancer types, ICR enabled (i.e. BRCA, SKCM, STAD, BLCA, SARC, HNSC, LIHC, UCEC), ICR disabled (UVM, PAAD, LGG, KIRC), and ICR neutral cancer types (ACC, CESC, CHOL, COAD, ESCA, GBM, KICH, KIRP, LUAD, LUSC, MESO, OV, PCPG, PRAD, READ, TGCT, THCA, THYM, UCS) in per cancer ICR cluster (*left panel*) and pan-cancer cluster setting (*right panel*). ICR: Immunologic Constant of Rejection.

Supplementary Figure 6: A. Boxplot showing mean ICR score for each cancer type per group of cancer types: ICR-enabled, ICR-neutral and ICR-disabled. A single dot represents a single cancer type. **B.** Boxplot showing delta between mean ICR score in ICR High cluster compared with mean ICR score in ICR Low cluster. A single dot represents a single cancer type. **C.** ICR coefficient of variations in relationship with ICR score according to cancer types. **D.** Distribution of ICR score within cancer types.

Supplementary Figure 7: Pan-cancer Kaplan-Meier curves in ICR-disabled (top left panel) and ICR-enabled (top right panel) groups and stratified analysis by AJCC pathologic stage I & II (middle panels) and stage III & IV (bottom panels).

Supplementary Figure 8: Dotted heatmap showing mean ES for each immune cell population per cancer type, mean ES scores were z-scored per row.

Supplementary Figure 9: A. Scatterplot of mean mutation rate versus mean neoantigen load per cancer type. **B.** Ratio of nonsilent mutation rate between ICR High and ICR Low groups versus the ratio of predicted neoantigen load between in ICR High compared to ICR Low groups. **C.** Ratio of nonsilent mutation rate between ICR High and ICR Low groups versus

mean nonsilent mutation rate. **D.** Ratio of predicted neoantigen load between ICR High compared to ICR Low groups versus mean predicated neoantigen load.

Supplementary Figure 10: A. Boxplot of ICR score by MSI status in COAD (left panel) and STAD (right panel). P-values of t-test to compare mean ICR score per MSI group are indicated in the plot. **B.** Boxplot of number of mutated genes with a negative coefficient in ICR trained elastic net model by MSI status in COAD (left panel) and STAD (right panel). P-values of t-test to compare mean number of mutations per MSI group are indicated in the plot.

Supplementary Figure 11: Table to check overlap between tumor intrinsic pathways genes and frequently mutated genes. When a gene (columns) is part of a gene signature (rows), this is indicated by “YES”, if not, it is indicated by “NO”. Genes that have a negative coefficient in trained model are shown in blue, pathways that inversely correlate with ICR (**Figure 2B**) are indicated in blue. Genes that have a positive coefficient in trained model are shown in red, pathways that positively correlate with ICR (**Figure 2B**) are indicated in red.

Supplementary Figure 12: A. Boxplot of ICR score by *PTEN* GISTIC CNV categories (deep deletion (-2), hemi-deletion (-1), wild-type (WT) (0), gain (+1), and amplification (+2) per cancer (*upper panel*) and pan-cancer (*lower panels*). **B.** Boxplot of ICR score by *PTEN* CNV categories by Log R ratio cut-off of -0.4, ≤ -0.4 CNV Low, and > -0.4 CNV High per cancer (*upper panel*) and pan-cancer (*lower panels*). **C.** Boxplot of ICR score by *PTEN* mutation status per cancer (*upper panel*) and pan-cancer (*lower panels*). Pan-cancer boxplots are plotted against ICR score (*left panels*) and ICR score that was mean centered by cancer type (*right panels*).

Supplementary Figure 13: A. Boxplot of ICR score by *CTNNB1* GISTIC CNV categories (deep deletion (-2), hemi-deletion (-1), wild-type (WT) (0), gain (+1), and amplification (+2) per cancer (*upper panel*) and pan-cancer (*lower panels*). **B.** Boxplot of ICR score by *CTNNB1* mutation per cancer (*upper panel*) and pan-cancer (*lower panels*). **C.** Boxplot of ICR score by status of *CTNNB1* mutation in exon 3 per cancer (*upper panel*) and pan-cancer (*lower panels*). Pan-cancer boxplots are plotted against ICR score (*left panels*) and ICR score that was mean centered by cancer type (*right panels*).

Supplementary Figure 14: Scatterplots of each of the combinations of: 1) ICR scores, 2) proliferation ES, 3) TGF- β signaling ES, and 4) mutation rate (n = 4452). Pearson's correlation coefficient and regression line (red) are indicated in the plots.

Supplementary Figure 15: Pan-cancer Kaplan Meier curves of ICR groups stratified by both Proliferation High (left panels) and Proliferation Low (right panels) groups (corresponding to classification of shown in **Figure 6A**) and by Mutation rate High (top panels) and Mutation rate Low (bottom panels) based on pan-cancer median mutation rate.

Supplementary Figure 16: Survival analysis of ICR Low versus ICR High in pathway enrichment categories across 40 pathway signatures (rows) for each cancer type (columns). HRs (hazard ratios) for death in high enrichment categories (**A**) are compared with HRs in low enrichment categories (**B**). **C.** Differences in prognostic impact of ICR classification between pathway signature enrichment categories for each cancer type. HR of ICR Low vs. ICR High was calculated per category from binary classification of enrichment of oncogenic pathway signatures (rows) within individual cancer types (columns). The delta between HR in the highly enriched group and the HR in the group with low enrichment was calculated for each signature/cancer type combination.